Supporting Information

Smart Excimer Fluorescence probe for visual Detection, Cell Imaging and Extraction of Hg^{2+}

Syed S. Razi, Rashid Ali, Priyanka Srivastava and Arvind Misra*

Department of Chemistry, Faculty of Science, Banaras Hindu University, Varanasi – 221 005. INDIA.

Corresponding author: arvindmisra2003@yahoo.com; amisra@bhu.ac.in
Tel: +91-542-6702503; Fax: +91-0542-2368127, 2368175.

Figure S1: ^{1}H NMR spectrum of **2** in DMSO-d_6.

Figure S2: FT-IR spectrum of **2**.

Figure S3: ^{13}C NMR spectrum of **2** in $CDCl_3$.

Figure S4: ESI-MS spectrum of **2**.

Figure S5: HRMS spectrum of **2**.

Figure S6: ^{1}H NMR spectrum of **3** in DMSO-d_6.

Figure S7: FT-IR spectrum of **3**.

Figure S8: FT-IR spectrum of **4**.

Figure S9: Change in (a) absorption and (b) emission spectra of **2** (10 μM) upon interference of competitive metal ions (20 equiv) in phosphate buffer (10 mM pH 7.0; 10% aqueous ACN, v/v). Bar plots.

Figure S10: Changes in fluorogenic response of **2**+Hg^{2+} (10 μM) upon interference of different metal ions (2.0 equiv) in phosphate buffer (10 mM pH 7.0; 10% aqueous ACN, v/v).

Figure S11. Change in the emission spectra of **2** by the addition of (a) EDTA to **2**+Hg^{2+} and (b) Hg^{2+} to **2** + EDTA in phosphate buffer (10 mM; pH 7.0; 10% aqueous ACN).

Figure S12: Fluorescence excitation spectra of **2** and **2**-Hg^{2+} upon excitation at (a) 397 and (b) 506 nm in phosphate buffer (10 mM; pH 7.0; 10% aqueous ACN).

Figure S13: Job's plot analysis based on (a) absorption and (b) emission spectra of **2**.

Figure S14: Relative change in (a) absorption and (b) emission spectra of **2** at different pH in phosphate buffer. Inset: A pH-absorption plot shows change in absorption of **2** at pH 8 to 14.

Figure S15: ^{1}H NMR titration spectrum of **2** upon addition of 0.5 equiv of Hg^{2+} in DMSO-d_6.

Figure S16: ^{1}H NMR titration spectrum of **2** upon addition of 1.0 equiv of Hg^{2+} in DMSO-d_6.

Figure S17: ^{1}H NMR titration spectrum of **2** upon addition of 1.5 equiv of Hg^{2+} in DMSO-d_6.

Figure S18. FT-IR spectrum of **2** and **2**-Hg^{2+} complex.

Figure S19: HRMS spectrum of **2-Hg^{2+}**complex.

Figure S20. SEM images showing morphology of aggregates of **4** (10μM) (a) without treated with Hg^{2+}, (b) and (c) with Hg^{2+}.

Figure S21. AFM images showing morphology of 2D and 3D aggregates of **4** (10 μM) without treated with Hg^{2+} (a, b, c) and with Hg^{2+}(d, e, f).

Figure S22: Change in (a) absorption and (b) emission spectra of **4** (10 μM) upon addition of competitive metal ions (20 equiv) in phosphate buffer (10 mM pH 7.0; 10% aqueous ACN, v/v).

Figure S23: Change in (a) absorption (b) emission titration spectra of **4** (10 μM) upon addition of Hg^{2+} (0-2 equiv) in phosphate buffer (10 mM pH 7.0; 10% aqueous ACN, v/v). Benesi-Hildebrand plots based on (c) absorption and (d) emission spectra.

Figure S24. Change in emission titration spectra upon addition of Hg^{2+} to a solution of BSA (λ_{ex} 278 nm) in NaOAc buffer (50 mM; pH 6.7).

Figure S25. (a) Dependence of fluorescence intensity of **2** on BSA (0.0- 3.0 μM) and (b) Change in fluorescence spectra of **2** upon addition of BSA (2 μM) and Hg^{2+} (2.0 equiv) in phosphate buffer (10 mM pH 7.0; 10% aqueous ACN).

Figure S26: (a) Calibration curve between relative emission intensities and different concentration of probe **2** and (b) calibration sensitivity (m) plots of human blood serum containing **2** + **Hg^{2+}** (10 μM) in phosphate buffer (10 mM; pH 7.0; 10% aqueous ACN).

2.1. General:

2.1.1. Materials and Chemicals. Reagents and solvents were purchased from Merck and Sigma-Aldrich and were used without any further purification. FT-IR spectra in KBr were recorded on a Varian-3100 FT-IR spectrometer. ^{1}H and ^{13}C NMR spectra (chemical shifts in δ ppm) were recorded on a JEOL AL 300 FT–NMR (300 MHz) spectrometer, using TMS as internal standard. The UV-Vis absorption spectra were recorded on Perkin Elmer 1700 spectrophotometer using a quartz cuvette (path length = 1cm). Fluorescence spectra were recorded on a Cary Eclipse fluorescence spectrophotometer (Varian). Stock solution of **2** (c = $1x10^{-3}$ M) was prepared in phosphate buffer (10 mM pH 7.0; 10% aqueous ACN). For absorption and emission experiment 100 μL and 10 μL of stock solution was taken and diluted to make the concentrations 10 μM and 1μM in a 3 mL probe solution. For interaction studies 0.1 M solutions of different metal ions was used. For ^{1}H NMR titration experiment solution of probe (1.02×10^{-2} M) and $HgClO_4$ was prepared in DMSO-d_6.

Moreover, to carryout experiments in biological medium, the human blood plasma (HSA) has been obtained, with due permission from Institute of Medical Sciences, Banaras Hindu University, Varanasi UP India. All experiments were performed in compliance with the relevant laws and institutional guidelines and the institutional committee has given consent for the same.

2.1.2. Estimation of Quantum Yields. The quantum yield of probe **2** and its complex, **2**-Hg^{2+} with respect to standard Quinine sulfate (Φ = 0.54, 1M H_2SO_4) have been estimated in phosphate buffer by the secondary method, using equation (1). The absorption and emission spectra of probe **2** and its complex **2**-Hg^{2+} were acquired under similar experimental condition of fluorescence standard (Quinine sulfate) to estimate their respective quantum yields with reference fluorophore.

$$\mathbf{Q = Q_R . I/I_R . OD_R/OD . n^2/n^2_R} \quad \mathbf{(1)}$$

Where Q is the quantum yield, *I* stand for integrated area of fluorescence intensities, OD is optical densities and *n* is the refractive indexes of solution. The subscript *R* refers to the reference fluorophore of known quantum yield.

2.1.3. Estimation of Binding Constant and Limit of detection. The binding constant for a 2:1 stoichiometry between **2** and Hg^{2+} was calculated by Benesi-Hildebrand method[30] using equation (2).

$$\mathbf{1 / (\mathit{I} - \mathit{I_o}) = 1 / (\mathit{I} - \mathit{I_f}) + 1 / \mathit{K} (\mathit{I} - \mathit{I_f}) [Hg^{2+}]^{1/2}} \quad \mathbf{(2)}$$

Where *K* is the association constant, *I* and I_o are the intensities of **2**, and of a complex, **2**+$\mathbf{Hg^{2+}}$, I_f is the maximum emission at saturation point.

The limit of detection (LOD) of **2** for Hg^{2+} was estimated by equation (3).

$$\mathbf{LOD = 3\sigma (}\text{standard deviation for }\mathbf{2) / m (}\text{calibration sensitivity)} \quad \mathbf{(3)}$$

Synthesis of Probe

Probe 2. To a solution of pyrene carboxaldehyde (0.232 g, 1.0 mmol) in anhydrous ethanol (8 ml) and a catalytic amount of acetic acid, ethanolamine (0.91 µl, 1.5 mmol) were added and the reaction mixture was refluxed for 2h. After the complete chemical reaction (monitored on TLC), the reaction mixture was cooled down to room temperature for precipitation, and filtered. The precipitate was washed with cold ethanolic solution and dried in air. Finally the desired compound was eluted by column chromatography using Hexane/Ethylacetate (5%) as solvent to get a yellow color crystalline solid in 78% yield. Mp. > 200^0C; R_f = 0.45 (EtOAc : hexane : : 4 : 6), IR (KBr) V_{max} (cm^{-1}) 3439, 2943, 1631, 1594, 1435, 1368, 1255, 1077, 846, 759, 676, 529, 440; ^{1}H NMR (DMSO-*d6*) d (ppm): 9.34 (s, 1H, N = CH), 9.12 (d, 1H, *J* = 9.6

Hz, pyrenyl), 8.56 (d, 1H, J = 7.8 Hz, pyrenyl), 8.36 (m, 7H, pyrenyl), 4.73 (t, J_1 = 5.1 Hz, J_2 = 5.4 Hz, OH), 3.87 (dd, 4H, J_1 = 4.8 Hz, J_2 = 5.4 Hz, CH_2); ^{13}C NMR (75 MHz, $CDCl_3$) d (ppm): 161.83, 131.23, 128.75, 128.68, 127.41, 126.21, 125.97, 125.70, 124.92, 122.38, 64.20, 62.70; ESI-MS; m/z at 274.1 $(M+H)^+$. HRMS (ESI-TOF) m/z: $[M]^+$ calculated 273.1153 and found 273.1156.

2.1.6. Synthesis of Probe 3: To a solution of **2** (68mg, 0.25mmol) in dry dichloromethane (3ml) N,N-diisopropylethylamine (0.5ml), 3-chloropropyl triethoxysilane (120µl, 0.5 mmol) were added and the reaction mixture was stirred for two days at room temperature. After the complete chemical reaction (monitored on TLC) the reaction mixture was concentrated in vacuum. The crude product was washed with ether and dried in air to obtain a yellow color semisolid in 72% yield. R_f = 0.45 (ethylacetate : hexane : : 4 : 6). IR (KBr) V_{max} (cm^{-1}) 2976, 1626, 1441, 1167, 1081, 958, 793, 688, 648, 469; ^1H NMR ($CDCl_3$) (ppm): 9.36 (s, 1H, -N=CH), 8.84 (d, 1H, J=9.3 Hz, pyrenyl), 8.55 (d, 1H, J = 8.1 Hz, pyrenyl), 8.31 (m, 9H, pyrenyl), 3.85 (m, 4H, CH_2), 3.55 (t, 2H, J_1 = 6.6 Hz, J_2 = 6.9 Hz, CH_2), 1.93 (t, 3H, J_1 = 6.9 Hz, J_2 = 8.4 Hz, CH_2), 1.24 (m, 11H, CH_2), 0.78 (m, 4H, CH_3).

2.1.7. Synthesis of Probe 4: To a solution of **3** (50 mg, 0.25 mmol) in dry dichloromethane (3 ml) silica gel (100-200 R) (50 mg) was added and the reaction mixture with stirred for 48h at room temperature. After the complete chemical reaction, the reaction mixture was concentrate in vacuum. The crude precipitate was washed with dry ether and dried gently in vacuum to obtain an orange color solid material in 68% yield. IR (KBr) V_{max} (cm^{-1}) 3444, 2925, 1644, 1509, 1156, 1089, 848, 759,711, 484.

Live cell imaging and Cell Viability (MTT assay) Experiment: HeLa cells were cultured in DMEM (Dulbeco's Modified Eagle Medium) supplemented with 10%

FBS (Fetal Bovine Serum), 1% antibiotics and antimycotic (Himedia) and incubated overnight at 37^{o}C in the environment of CO_2 (5%) as per manufacturer's protocol. Probe **2** (30 μM) was dissolved in a cultured medium containing 0.1% (V/V) DMSO and incubated in the HeLa cells for 30 min at 37 °C. As a control experiment, the cells were pretreated with PBS or N-methylmaleimide (NMM, 500 μM) for 1h then, washed (5 min, two times) with 1X PBS buffer (pH 7.4) and incubated with **2** (10, 20, 30, 40, 50 μM) in the cultured media containing 0.1% (V/V) DMSO. After 30 min of incubation cell images were acquired under a fluorescence microscope.

To study the cytotoxic tolerance, HeLa cells were seeded in 96-well plates (5 x 10^3 cells/ well) in duplicate and were cultured in complete DMEM medium. HeLa cells were incubated separately with different concentration of probe **2** (10, 20, 30, 40, 50 μM) and probe **2** with $HgNO_3$ (1μM) for 24h. To determine cell viability, the colorimetric metabolic activity assay was performed by incubating treated cells with 3-(4,5-dimethylthiazol-2-yl)-3,5-diphenyltetrazolium bromide (MTT) (5 mg/mL MTT reagent in PBS) for 2h. The insoluble purple formazan crystals, obtained by the reduction of yellow tetrazolium salt (MTT) on metabolically active cells, were dissolved with the help of DMSO (Sigma). The color was quantified spectrophotometrically on a microtiter plate reader (Bio-Rad model 680 microplate reader) at 380 nm excitation. Each experiment was repeated for three times. The cytotoxic effect of the probe was assessed through the ratio of the absorbance of the probe treated sample versus the control sample. The confocal microscopic images were recorded on LSM 510 Meta Confocal microscope (20X Zeiss objective lens). To collect confocal microscopic images HeLa cells were treated separately with 30 μM solution of probe **2** and **2**+$HgNO_3$ in dark and washed twice for 5 min with 1X PBS

buffer (Phosphate saline, pH 7.4). Cells were recollected by centrifugation (at 2000 rpm for 2 min) and mounted on slides with the help of DABCO.

Detection of Hg^{2+} in a real contaminated water samples: To accomplish, real crude water sample (50 mL) was passed through microfiltration membrane and the pH of the sample was adjusted using phosphate buffer. The aliquots of water samples were mixed with accurately prepared different concentration of Hg^{2+} (0.05, 0.5, 5 μM). The resulting samples then treated with **2** in phosphate buffer (pH, 7.0) to obtain final mixtures (3 mL) containing accurate concentration of probe **2** (10 μM) and Hg^{2+} (0.05, 0.5, 5 μM). The samples were left for 10 min and fluorescence spectra were measured in triplicates.

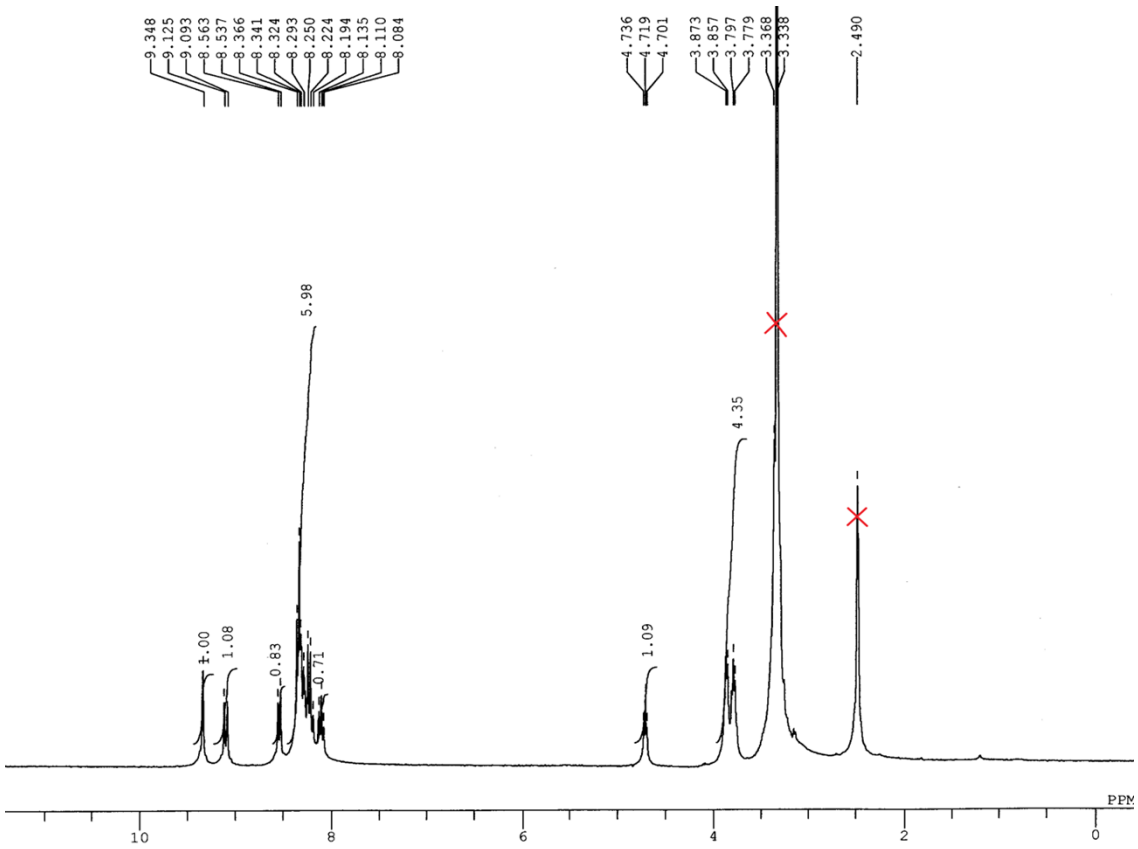

Figure S1: ^{1}H NMR spectrum of **2** in DMSO-d_6.

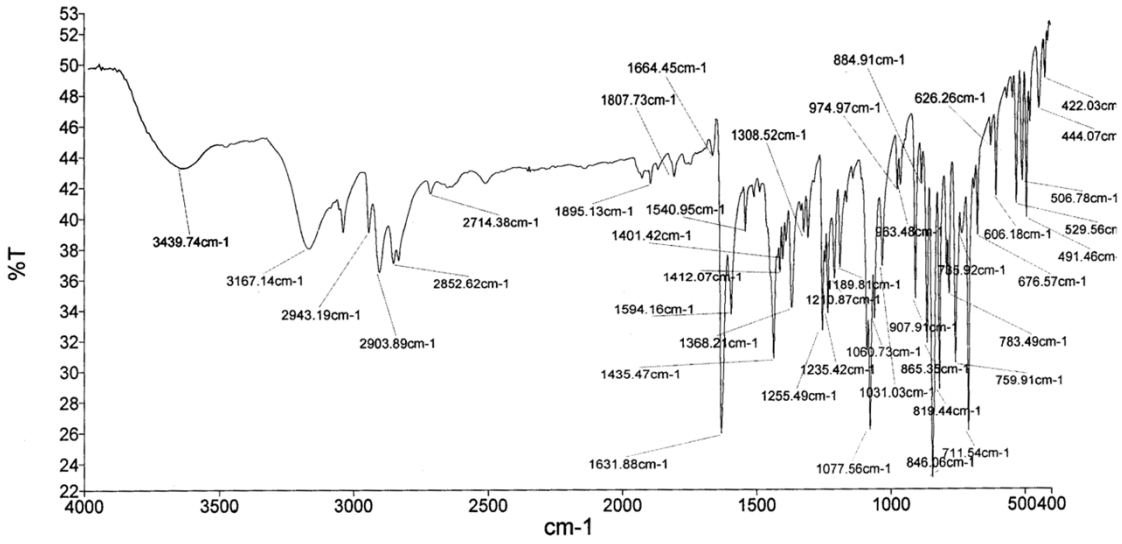

Figure S2: FT-IR spectrum of **2**.

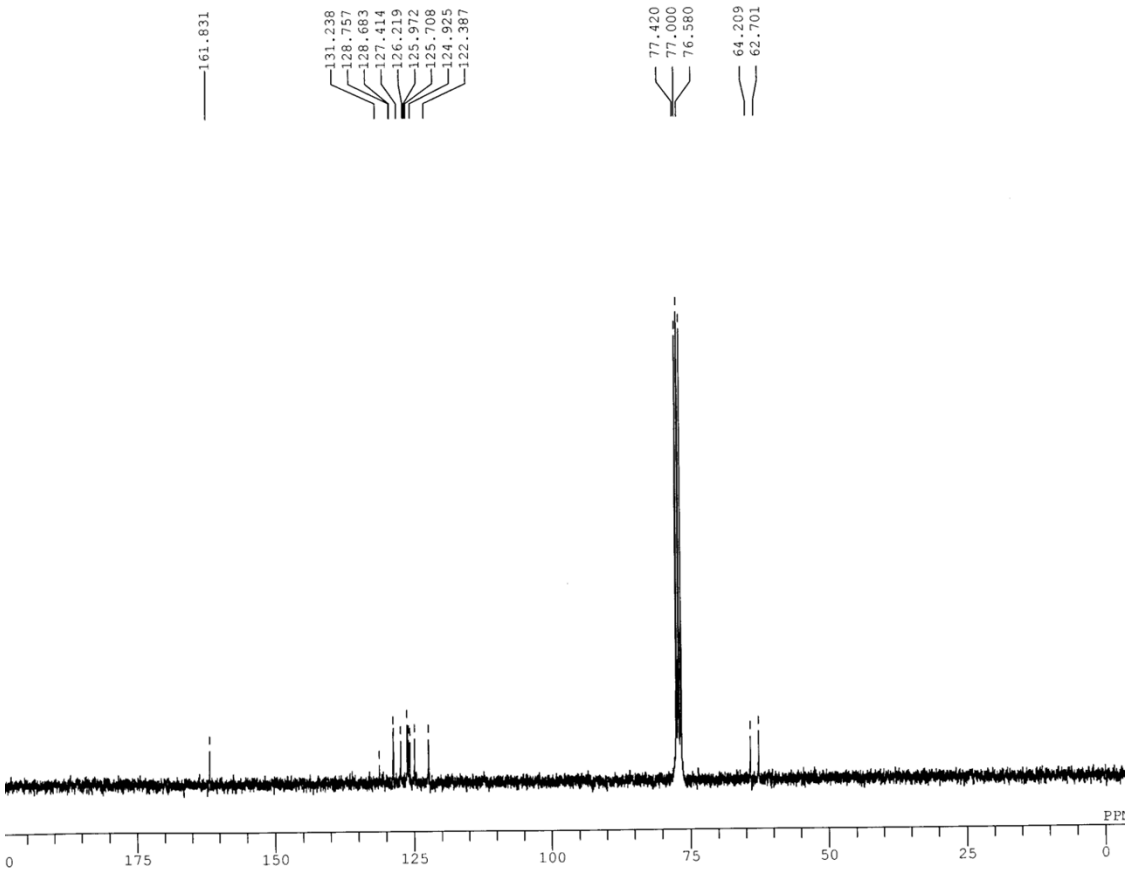

Figure S3: ^{13}C NMR spectrum of **2** in $CDCl_3$.

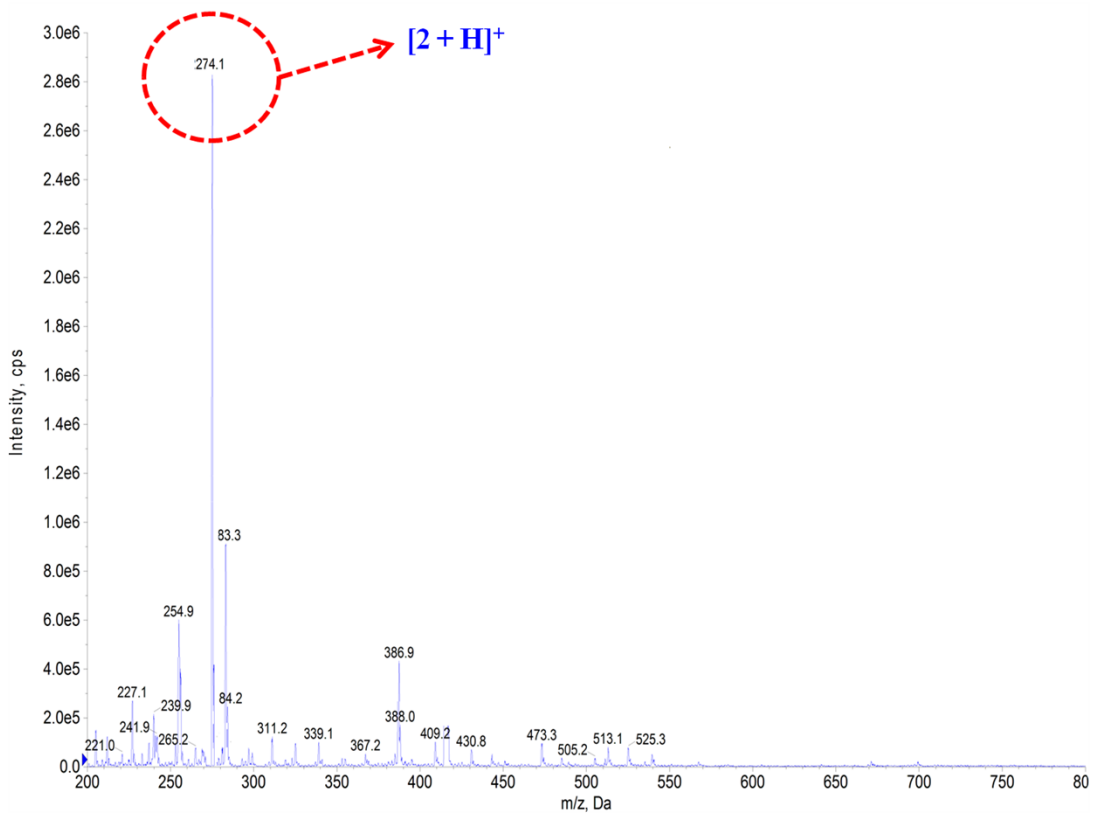

Figure S4: ESI-MS spectrum of **2**.

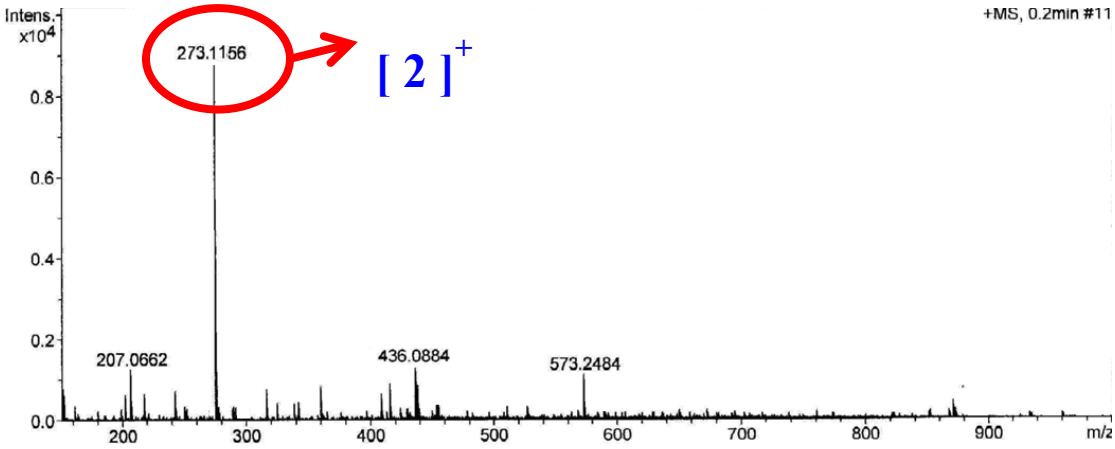

Figure S5: HRMS spectrum of **2**.

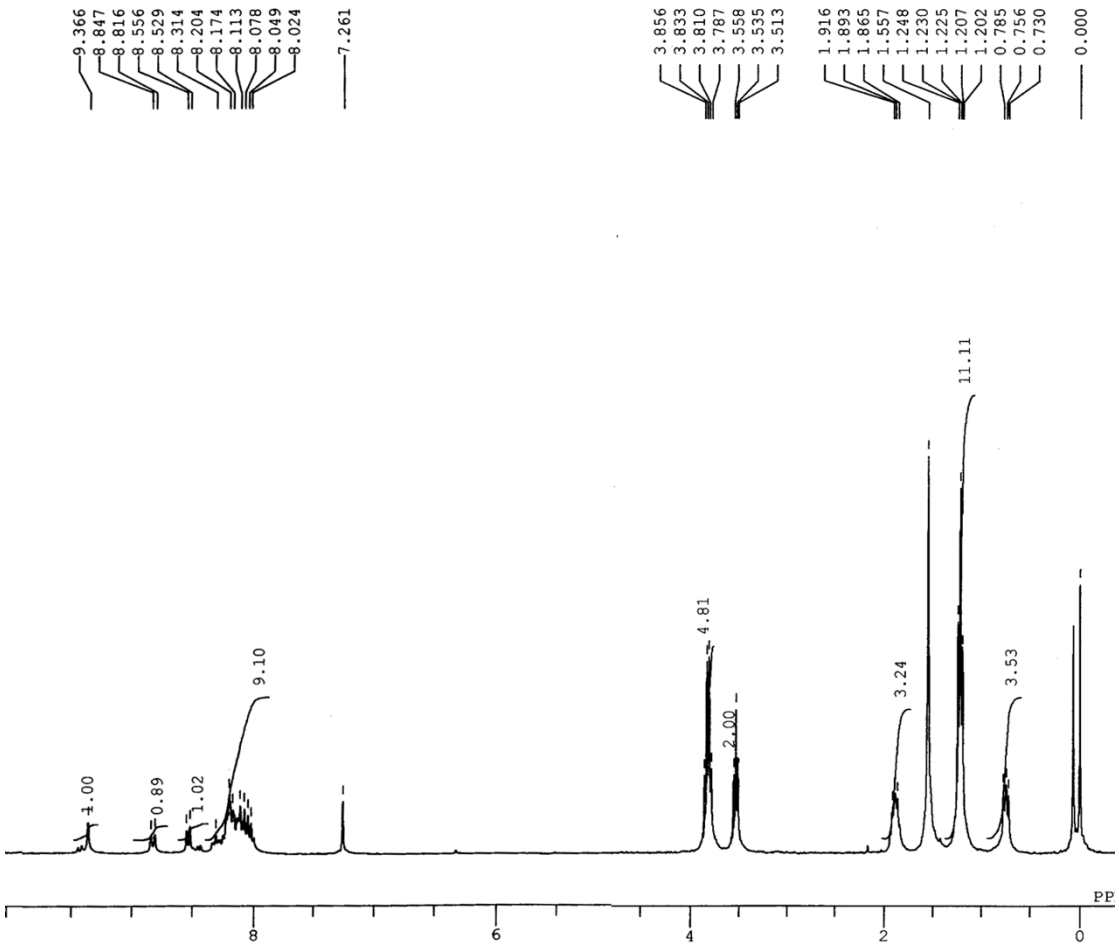

Figure S6: ^{1}H NMR spectrum of **3** in DMSO-d_6.

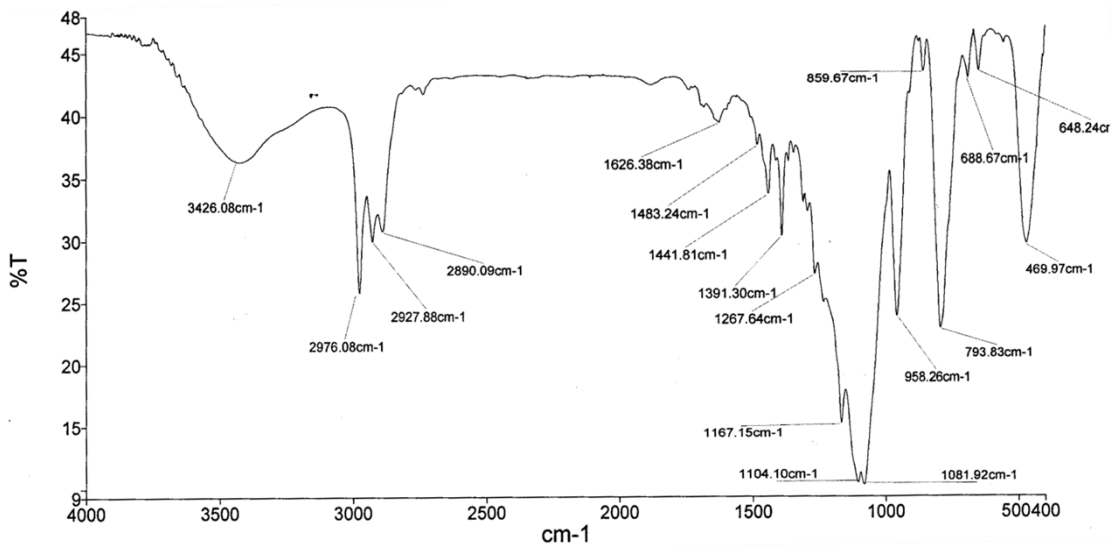

Figure S7: FT-IR spectrum of **3**.

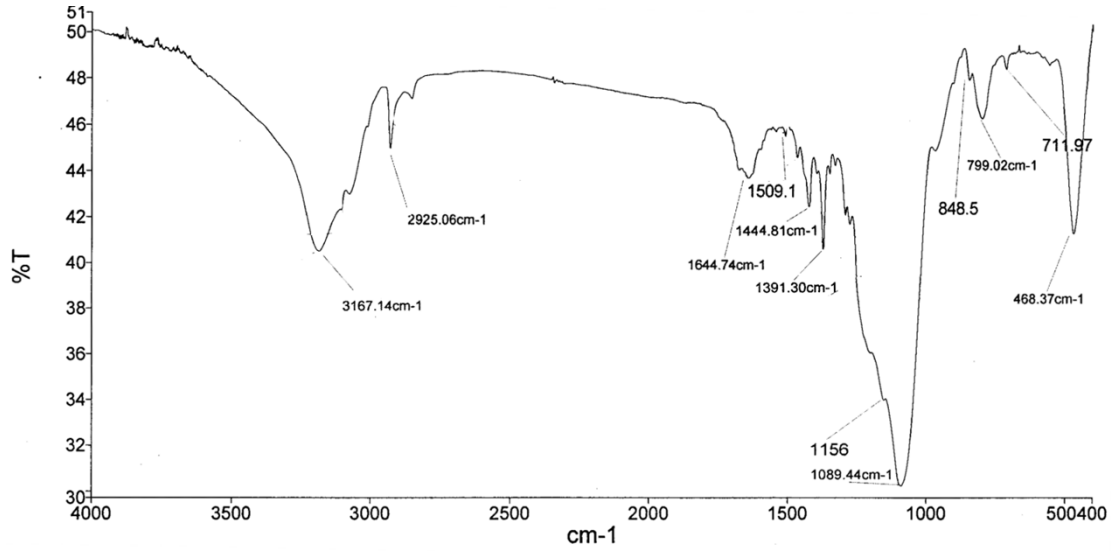

Figure S8: FT-IR spectrum of **4**.

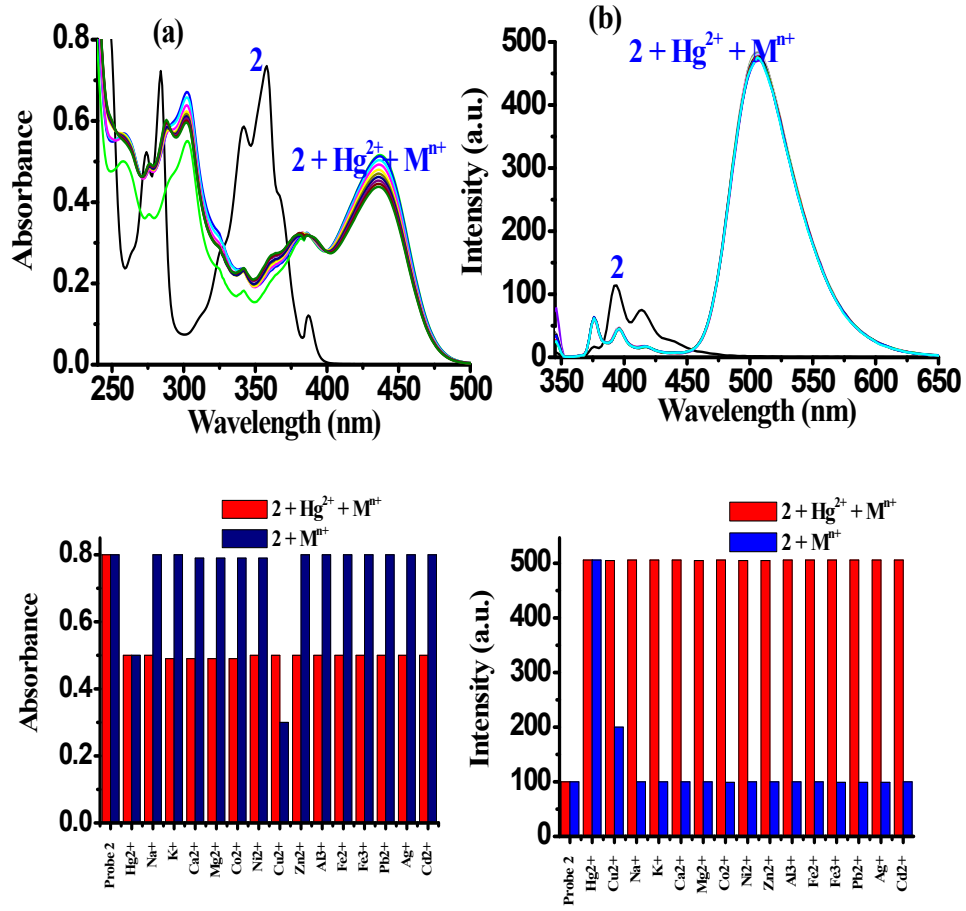

Figure S9: Change in (a) absorption and (b) emission spectra of **2** (10 μM) upon interference of competitive metal ions (20 equiv) in phosphate buffer (10 mM pH 7.0; 10% aqueous ACN, v/v). Bar plots.

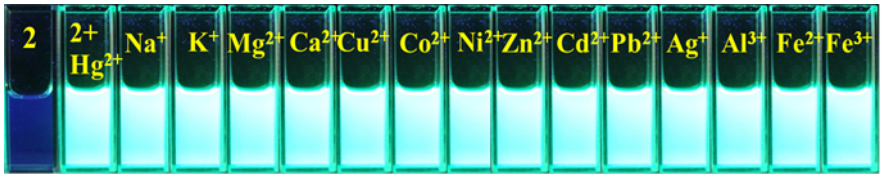

Figure S10: Changes in fluorogenic response of **2**+Hg^{2+} (10 μM) upon interference of different metal ions (2.0 equiv) in phosphate buffer (10 mM pH 7.0; 10% aqueous ACN, v/v).

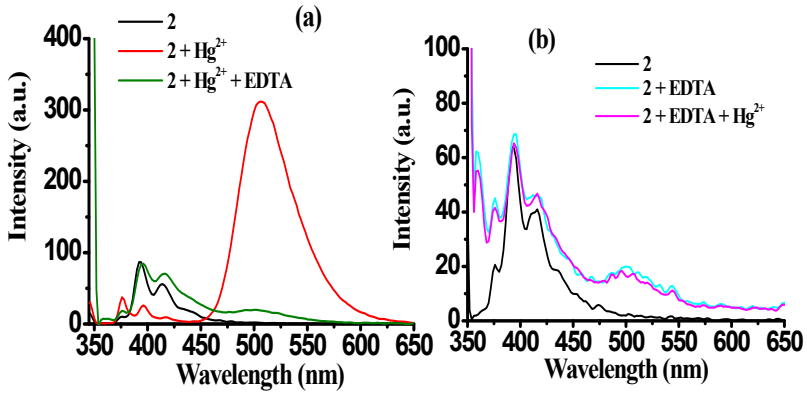

Figure S11. Change in the emission spectra of **2** by the addition of (a) EDTA to **2**+Hg^{2+} and (b) Hg^{2+} to **2** + EDTA in phosphate buffer (10 mM; pH 7.0; 10% aqueous ACN).

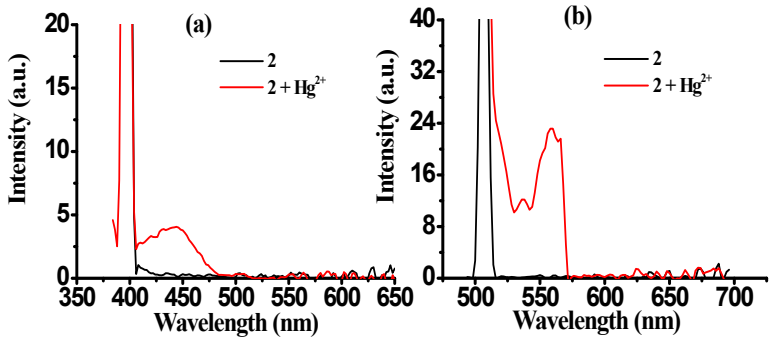

Figure S12: Fluorescence excitation spectra of **2** and **2**-Hg^{2+} upon excitation at (a) 397 and (b) 506 nm in phosphate buffer (10 mM; pH 7.0; 10% aqueous ACN).

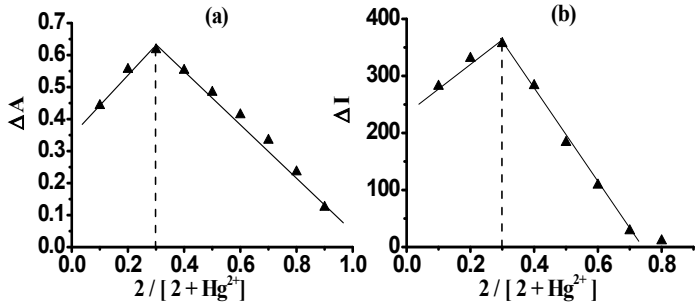

Figure S13: Job's plot analysis based on (a) absorption and (b) emission spectra of **2**.

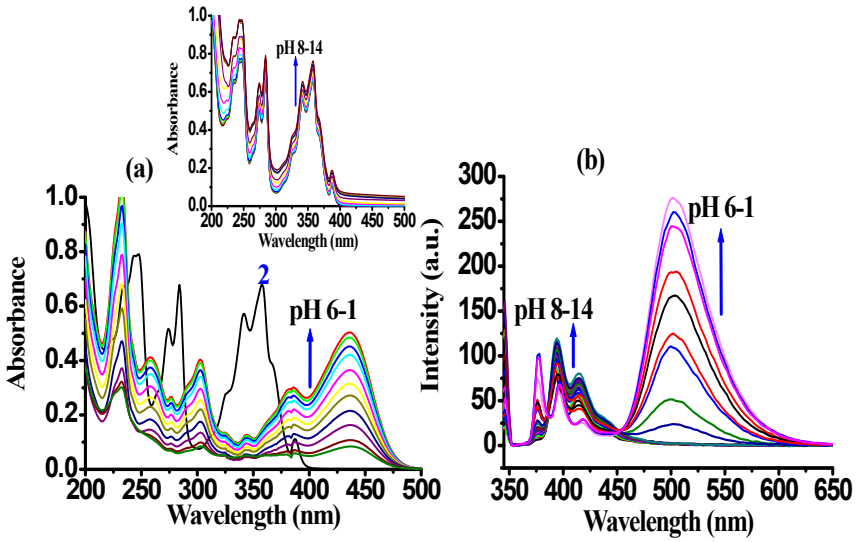

Figure S14: Relative change in (a) absorption and (b) emission spectra of **2** at different pH in phosphate buffer. Inset: A pH-absorption plot shows change in absorption of **2** at pH 8 to 14.

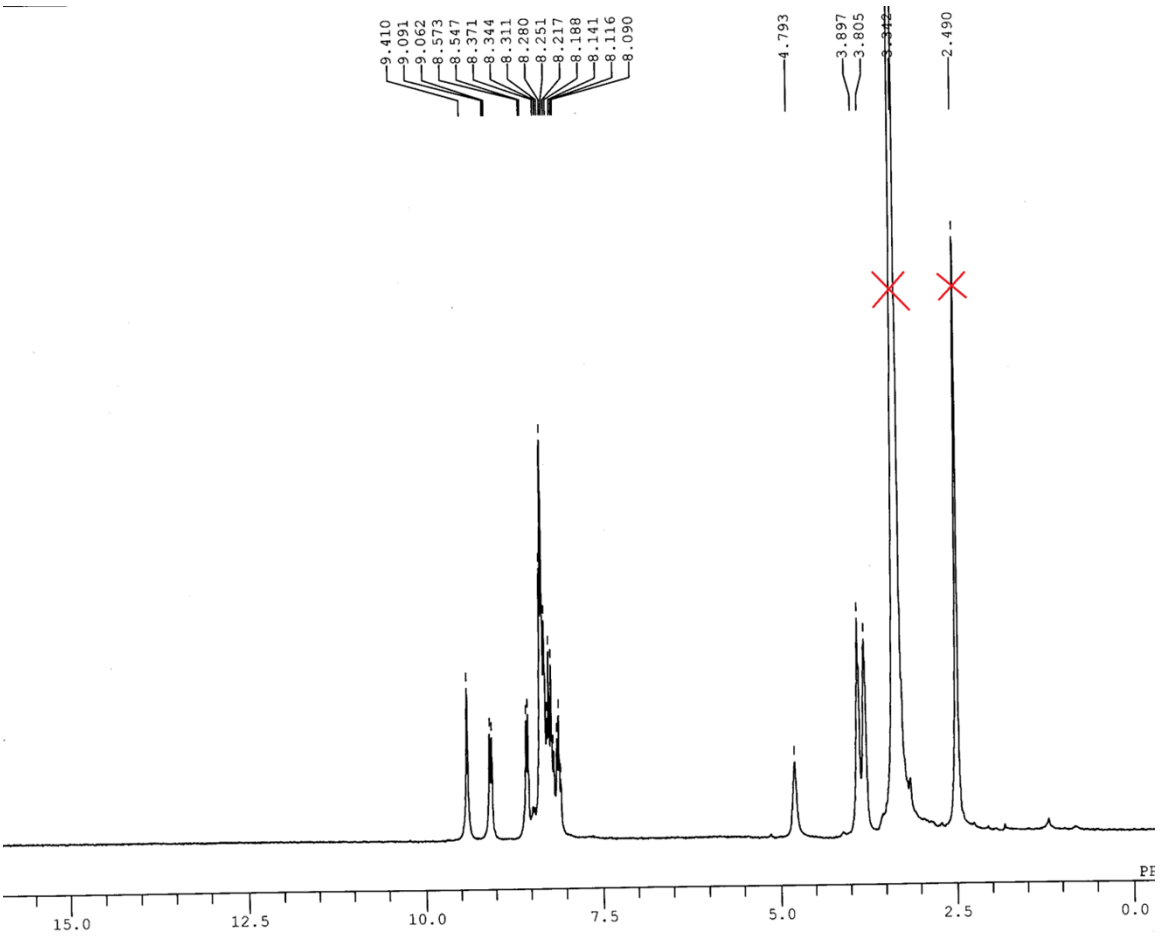

Figure S15: ^{1}H NMR titration spectrum of **2** upon addition of 0.5 equiv of Hg^{2+} in DMSO-d_6.

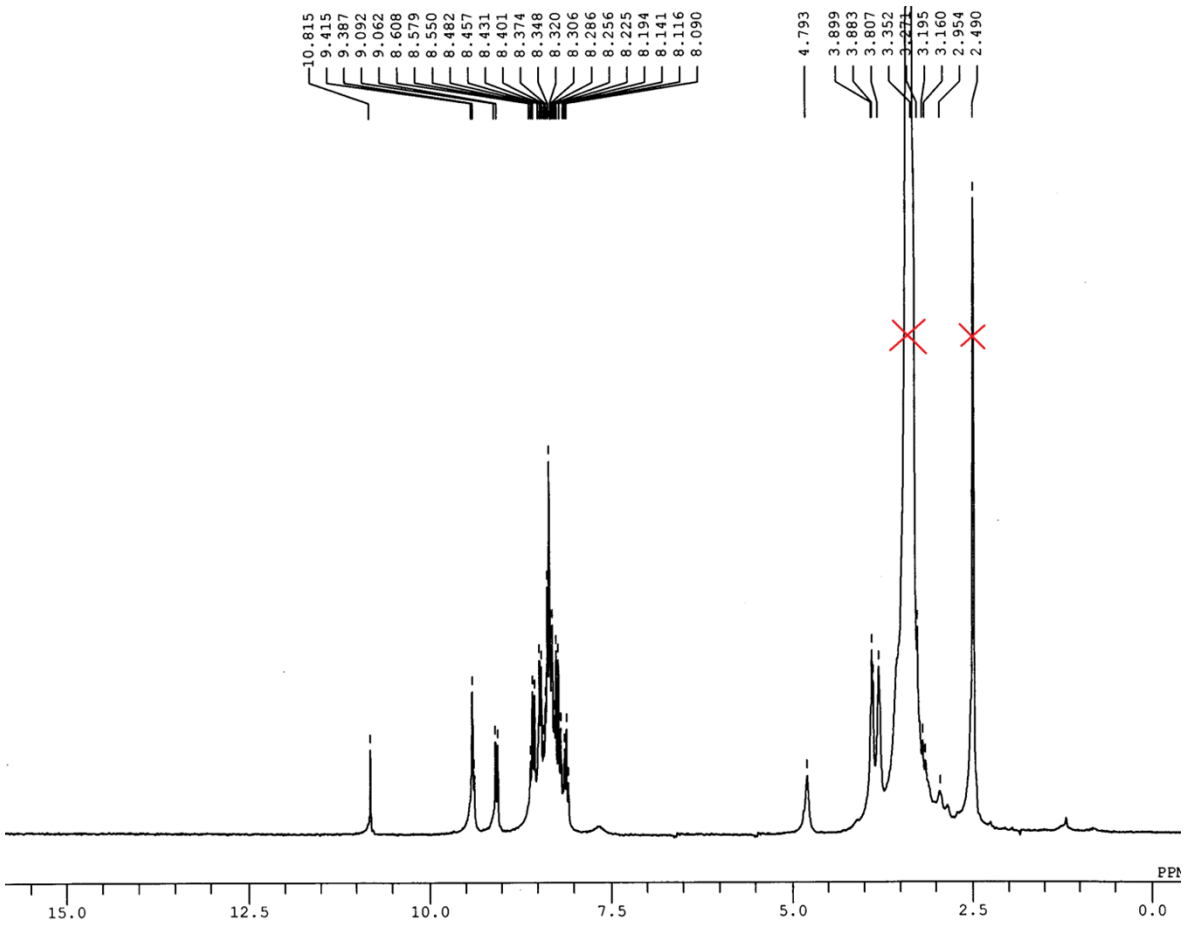

Figure S16: ^{1}H NMR titration spectrum of **2** upon addition of 1.0 equiv of Hg^{2+} in DMSO-d_6.

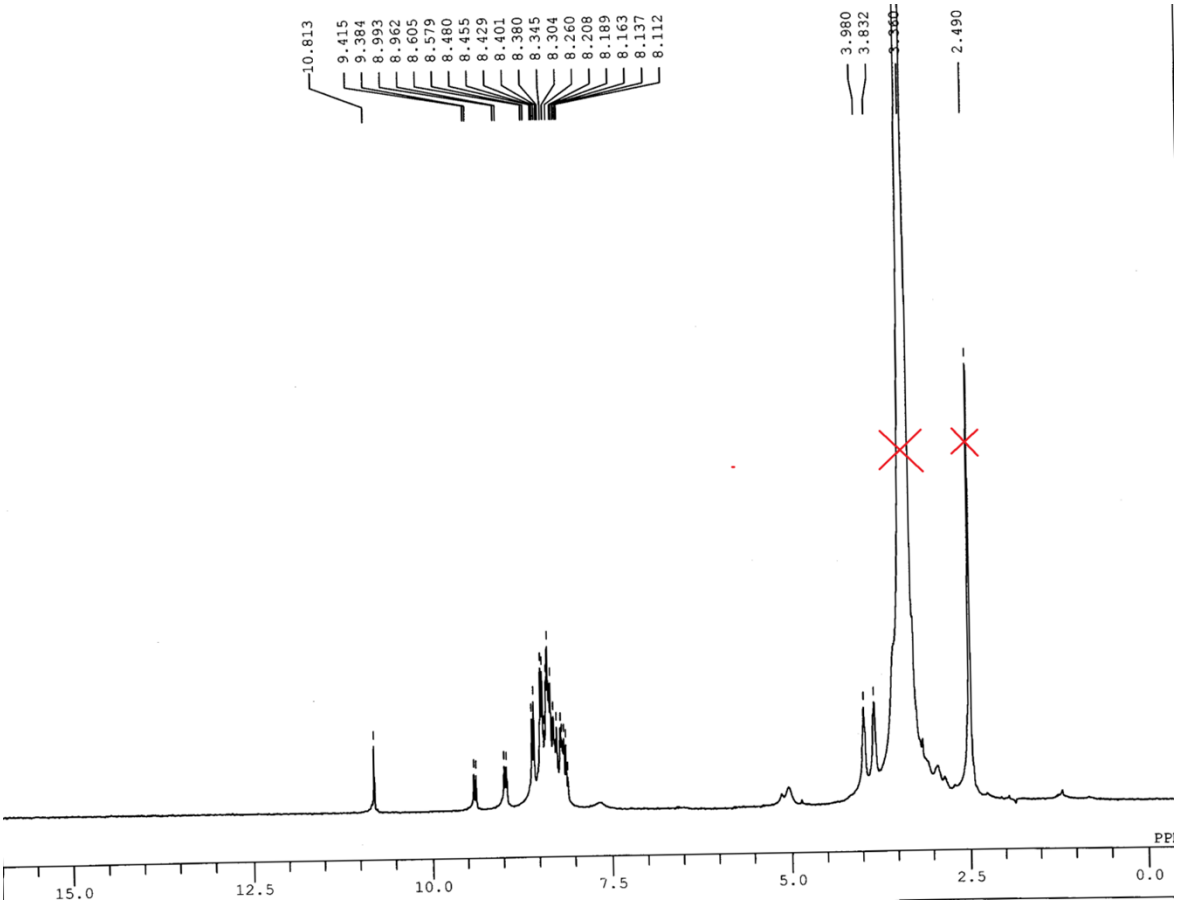

Figure S17: ^{1}H NMR titration spectrum of **2** upon addition of 1.5 equiv of Hg^{2+} in DMSO-d_6.

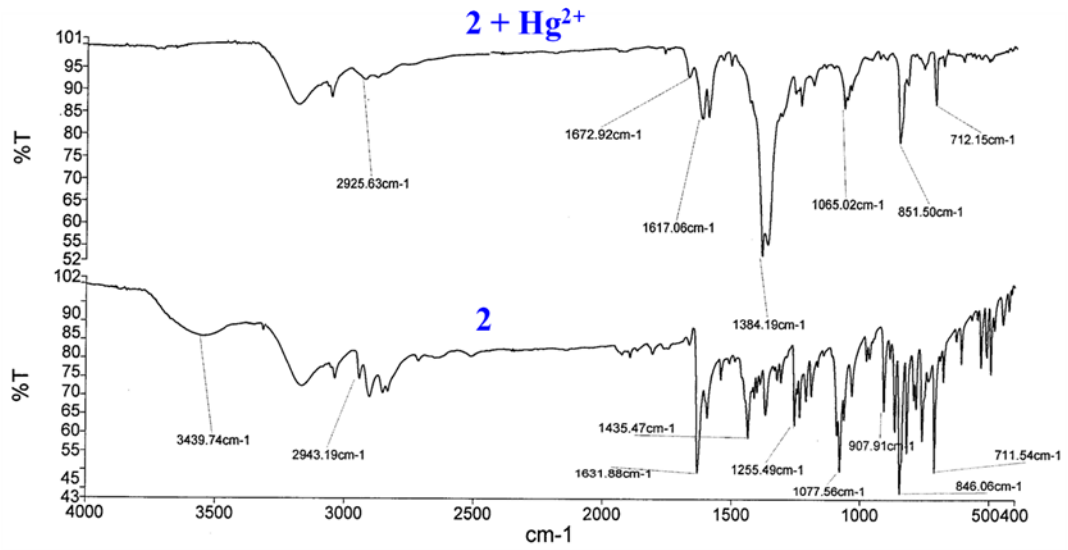

Figure S18. FT-IR spectrum of **2** and **2**-Hg^{2+} complex.

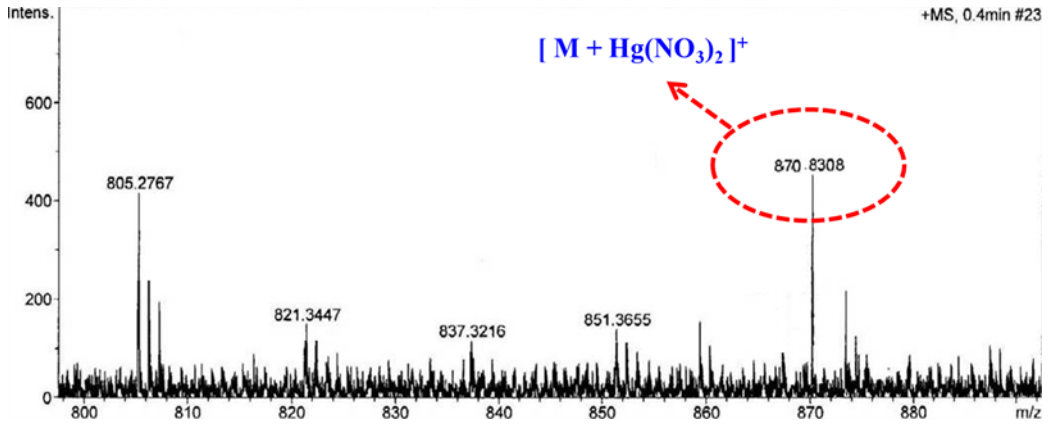

Figure S19: HRMS spectrum of **2-**Hg^{2+}complex.

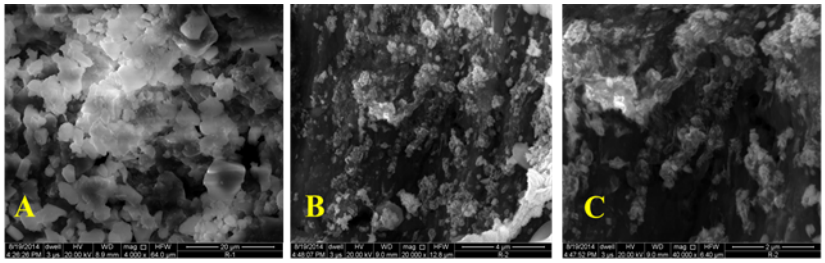

Figure S20. SEM images showing morphology of aggregates of **4** (10μM) (a) without treated with Hg^{2+}, (b) and (c) with Hg^{2+}.

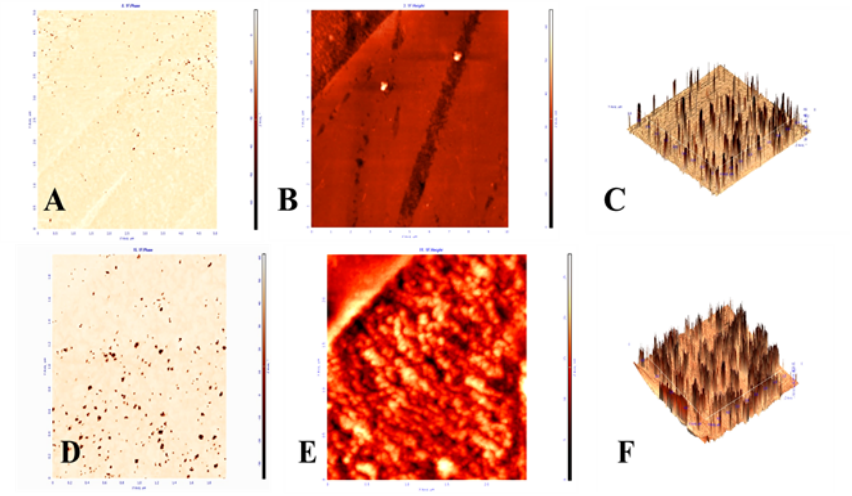

Figure S21. AFM images showing morphology of 2D and 3D aggregates of **4** (10 μM) without treated with Hg^{2+} (a, b, c) and with Hg^{2+}(d, e, f).

Competitive metal Ion Interaction studies of 4: The practical applicability of probe **4** as a selective fluorescent chemosensor for Hg^{2+} has been demonstrated by performing the competitive metal ion interference experiments. The tested cations (0-2 equiv) were added to a solution of probable complex, **4**+Hg^{2+} and reversibly by the addition of Hg^{2+} (0-2 equiv) to a solution of **4** (5 μM) containing excess of other metal ions (Figure S22). The absorption spectra upon addition of tested cations illustrated insignificant change in absorption bands of a complex **4**+Hg^{2+} (5 μM). Similarly, no

significant variation in emission behavior of **4** was observed in either condition. Thus, the experimental observation suggested that **4** may be utilized as a potential fluorescent optoelectronic material to detect Hg^{2+}. The appearance of new emission band of relatively high emission intensity signifies the formation of a new species in medium due to complexation of Hg^{2+} through the coordination site with *N* and *O* atoms of aldimine and etheral functional groups.

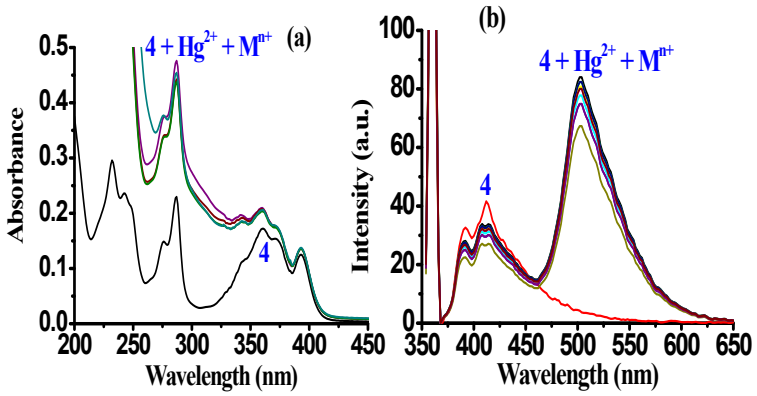

Figure S22: Change in (a) absorption and (b) emission spectra of **4** (10 μM) upon addition of competitive metal ions (20 equiv) in phosphate buffer (10 mM pH 7.0; 10% aqueous ACN, v/v).

Binding affinity of probe 4: The absorption titration experiment was performed to understand the binding affinity of **4** (5 μM) with Hg^{2+}. Upon sequential addition of Hg^{2+} (0–2 equiv) to a solution of **4** the broad band centered at 360 nm shifted with the formation of a new transition band at 357 nm (blue shift ~3 nm) and hyperchromic shift was observed at 286 nm gradually. An association constant estimated by Benesi-Hildebrand method[30] was found to be K_{assoc} = 3.60 x 10^6 $M^{-1/2}$ (Figure S23c). The fluorogenic affinity of **4** (5 μM) with Hg^{2+} was evaluated by fluorescence titration experiment (Figure S23). Upon increasing concentration of Hg^{2+} (0–2 equiv) to a solution of **4,** relative fluorescence intensity increased significantly at 502 nm with the

formation of an isoemissive point at 456 nm, and the estimated binding constant, from the fluorescence titration data was found to be 2.5 x 10^5 $M^{-1/2}$ (Figure S23d).

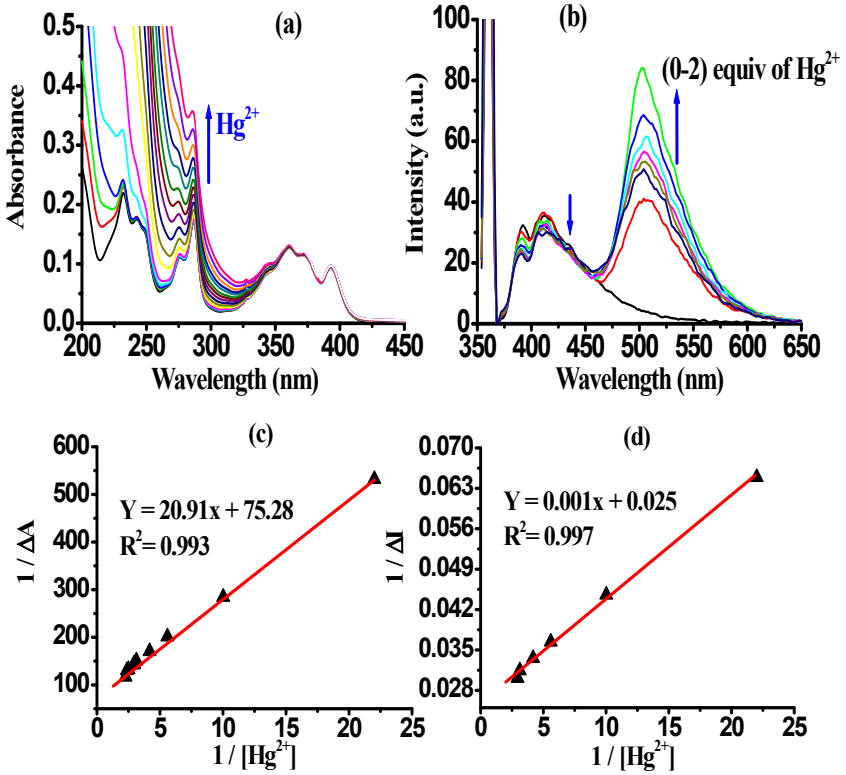

Figure S23: Change in (a) absorption (b) emission titration spectra of **4** (10 μM) upon addition of Hg^{2+} (0-2 equiv) in phosphate buffer (10 mM pH 7.0; 10% aqueous ACN, v/v). Benesi-Hildebrand plots based on (c) absorption and (d) emission spectra.

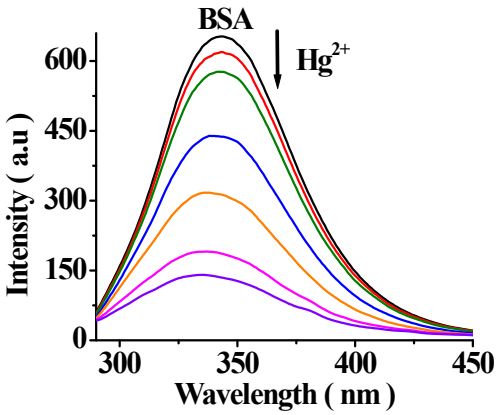

Figure S24. Change in emission titration spectra upon addition of Hg^{2+} to a solution of BSA (λ_{ex} 278 nm) in NaOAc buffer (50 mM; pH 6.7).

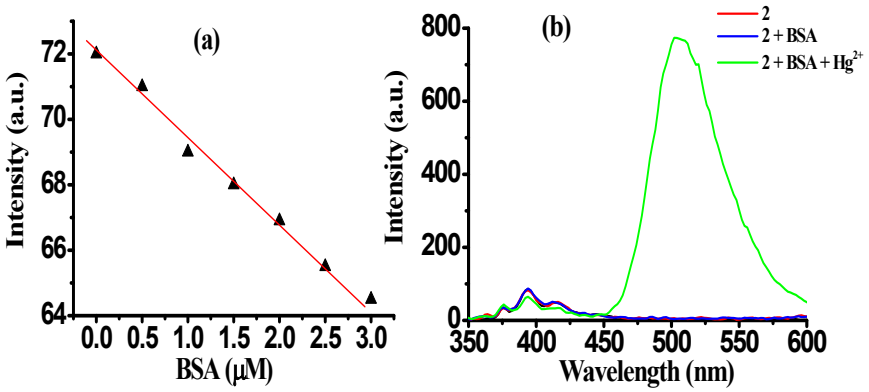

Figure S25. (a) Dependence of fluorescence intensity of **2** on BSA (0.0- 3.0 μM) and (b) Change in fluorescence spectra of **2** upon addition of BSA (2 μM) and Hg^{2+} (2.0 equiv) in phosphate buffer (10 mM pH 7.0; 10% aqueous ACN).

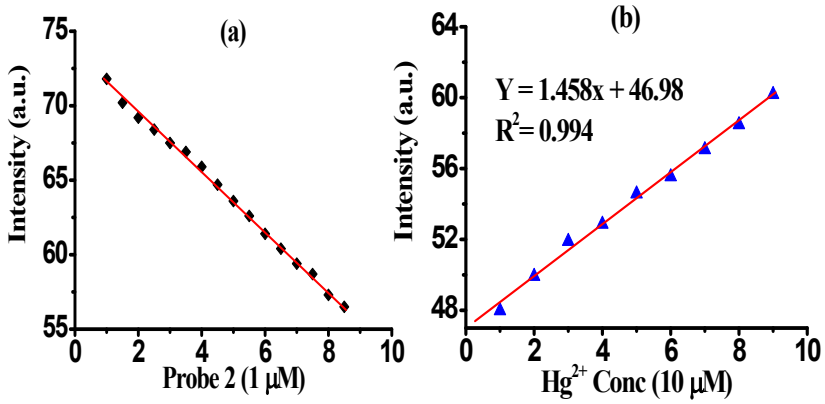

Figure S26: (a) Calibration curve between relative emission intensities and different concentration of probe **2** and (b) calibration sensitivity (m) plots of human blood serum containing **2** + **Hg^{2+}** (10 μM) in phosphate buffer (10 mM; pH 7.0; 10% aqueous ACN).